

Orbiting cross sections: Application to black hole scattering

P. Anninos,* C. DeWitt-Morette, R. A. Matzner, P. Yioutas, and T. R. Zhang[†]

Department of Physics, Center for Relativity, The University of Texas at Austin, Austin, Texas 78712-1081

(Received 24 February 1992)

The semiclassical formulas for orbiting cross sections (spiraling scattering) are derived for particles and for scalar waves. They are applied to scalar waves orbiting Schwarzschild black holes. The cross sections for scalar waves orbiting Schwarzschild black holes are also computed numerically by the method of partial wave decomposition. They are compared with the semiclassical analytic cross sections. The approximations made in the semiclassical analysis determine the scattering up to two parameters: the overall amplitude and the phase of the oscillation in the cross section. When matched to the amplitude and phase of the numerical computation there is an extremely close fit between the analytical and the numerical cross sections. Therefore we conclude that the oscillatory features observed in the numerical calculations away from forward- and backward-scattering angle are due to orbiting. Backward glory scattering has been computed analytically previously; the perfect agreement with the numerical results shows that the behavior of the cross section for a scattering angle $\theta \simeq \pi$ is due to glory scattering. Together these results interpret the numerically computed cross section for the entire range of scattering angles. The analytical calculation of the glory and orbiting cross sections is an application of the pre-distribution formulation of functional integration.

PACS number(s): 03.80.+r, 03.40.Kf, 03.65.Sq, 11.80.Et

I. INTRODUCTION

A. Orbiting

In particle scattering by a potential, it can happen that the particle orbits several times around the scattering center before escaping. This phenomenon is called orbiting, or spiral scattering. Orbiting cross sections have so far eluded analytical computation.

Orbiting is discussed by Ford and Wheeler [1,2] in their semiclassical description of quantum scattering. They “conclude that there is no semiclassical approximation to the orbiting effect of simplicity or generality comparable to the analysis for rainbow scattering and glory scattering,” and they “content [themselves] with mentioning several possible limiting situations”: the sharp spike of the deflection function, the thin or thick barrier of the effective potential in the radial wave equation. They apply these results to the scattering of α particles by nuclei and to the scattering of atoms by atoms [3].

Berry concludes his paper [4] on uniform approximations for glory scattering and diffraction peaks with these words: “All the common semiclassical potential scattering effects have been treated by methods of uniform approximation with the one exception of orbiting; the pioneer work of Ford and Wheeler (1959) has hardly been improved on, and a uniform approximate treatment is not yet in sight.”

The semiclassical calculations of orbiting cross sections

are difficult because orbiting contributes to all observation angles, and because an infinite number of classical paths contribute to the semiclassical cross section.

B. Glory and spiral scattering by black holes

More recently, Handler and Matzner [5] computed numerically the scattering cross section of gravitational waves by a Schwarzschild black hole. They suggested that the oscillatory dependence of the cross section on the scattering angle θ results from glory scattering interferences when $\theta \approx \pi$, and from orbiting interferences when θ is not necessarily close to π .

Their conjecture was proved to be correct in the case of backward scattering by DeWitt-Morette, Nelson, and Zhang who computed analytically the glory scattering cross section [6–9]: In Fig. 1 reproduced from [10] the solid line represents the numerical computation of the scattering of gravitational waves by a Schwarzschild black hole for $M\omega = 2.5$ where M is the mass of the black hole and ω the energy of the incoming wave. The dotted line is the analytically computed leading term $d\sigma_{\text{WKB}}^{\xi}$ in a high-frequency expansion¹ of the cross section for glory scattering in the solid angle $d\Omega$, in the θ direction, of polarized classical waves of energy $\omega = 2\pi\lambda^{-1}$, helicity

¹We label “WKB” all leading terms in high-frequency expansions because the high-frequency cross sections have been obtained from semiclassical expansions of quantum-mechanical cross sections—changing the scale indicator \hbar to a scale indicator ν^{-1} . It should also be noted that we are referring to *leading terms* in these approximations, not to the standard (strict) “WKB” approximations which are not valid here.

*Present address: National Center for Supercomputing Applications, University of Illinois, Champaign, Illinois 61820.

[†]Present address: Compact Software, Inc., Paterson, NJ 07504.

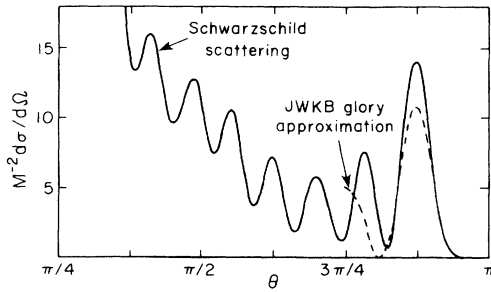


FIG. 1. Scattering of a gravitational wave of angular frequency ω by a Schwarzschild black hole of mass M , where $M\omega = 2.5$ (in units $G = c = 1$). The solid line is the cross section numerically computed by Handler and Matzner [2]. The dotted line is the glory cross section analytically computed by DeWitt-Morette, Nelson, and Zhang [3,4]. This reproduces Fig. 8.15 from [1]. In [1] the dotted glory cross section was incorrectly attributed, which we correct here.

$s = 2$, by a (long-range) central potential:

$$d\sigma_{\text{WKB}}^g = 2\pi\omega B_g^2 \left| \frac{dB}{d\theta} \right|_{\pi} J_{2s}^2(\omega B_g \sin \theta) d\Omega \quad \text{for } \theta \approx \pi, \quad (1.1)$$

where B_g is the glory impact parameter, defined by the deflection function $\Theta(B_g) = \pi$. For a Schwarzschild black hole of mass M the impact parameter $B(\theta)$ is given by the Darwin formula [11]

$$B(\theta) = [3\sqrt{3} + 3.48 \exp(-\theta)]M, \quad c = 1, \quad G = 1, \quad (1.2)$$

$$B_g = B(\pi) = 5.35.$$

The discrepancy between the dotted and solid lines is due to the fact that (1.1), valid for $\theta \approx \pi$, is plotted in the range $\frac{3}{4}\pi \leq \theta \leq \pi$ for a B with an exponential, θ dependence. It is clear from the $M\omega$ dependence of the cross section given in [10] that, if computed for larger values of $M\omega$ and for θ closer to π , the fit between the solid and dotted lines would be near perfect.

One wishes to investigate the reasons for the oscillations of the cross section for all values of θ , and ascertain whether or not they are due to orbiting.

In particle scattering, orbiting occurs [1,2] when the deflection function $\Theta(l)$ as a function of the angular momentum l has a logarithmic singularity at $l = \bar{l}$:

$$\Theta(l) = \begin{cases} \theta_1 + b \ln[(l - \bar{l})/\bar{l}] + \dots & \text{for } l > \bar{l}, \\ \theta_2 + 2b \ln[(\bar{l} - l)/\bar{l}] + \dots & \text{for } l < \bar{l}, \end{cases} \quad (1.3a)$$

$$(1.3b)$$

for some constants θ_1 , θ_2 , and b . Large values of $\Theta(l)$ mean that the particle orbits several times around the scattering center before escaping. For $l = \bar{l}$ the particle is trapped in orbit. The logarithmic behavior of the deflection function occurs when the energy of the incoming particle is close to a local maximum of the effective potential of the radial wave function [9].

Darwin [11] has shown that, in the neighborhood of a

Schwarzschild black hole, a massless particle (incoming null ray) with the impact parameter $\bar{B} = 3\sqrt{3}M$ is trapped by the black hole and spirals toward a limiting circular orbit of radius $3M$. In terms of the angular momentum $l = B$ [initial momentum] = $B\omega = B\omega$, the Darwin formula (2.2) can then be written

$$l(\theta) = [\bar{l} + 3.48 \exp(-\theta)]M\omega, \quad (1.4a)$$

$$\Theta(l) = -\ln(3.48M\omega/\bar{l}) + \ln[(l - \bar{l})/\bar{l}]. \quad (1.4b)$$

The Darwin formula exhibits the logarithmic singularity responsible for particle orbiting.

Classical waves are said to be orbiting if the characteristic system of their eikonal equation defines a flow which includes orbiting paths. Therefore the presence of orbiting can be predicted from the effective potential which enters the radial wave equation. The radial wave equation for a scalar wave [12],

$$\phi = \exp(i\omega t) R_{l\omega}(r) Y_l^m(\theta, \varphi),$$

$$Y_l^m = \text{spherical harmonic}, \quad (1.5)$$

scattered by a Schwarzschild black hole, i.e., propagating in a manifold with the metric

$$ds^2 = -(1 - 2M/r)dt^2 + (1 - 2M/r)^{-1}dr^2 + r^2 d\Omega^2,$$

$$d\Omega^2 = r^2 d\theta^2 + r^2 \sin^2\theta d\phi^2 \quad (1.6)$$

is

$$\left[\frac{d^2}{dr^{*2}} + \omega^2 - \left(1 - \frac{2M}{r} \right) \left(\frac{2M}{r^3} + \frac{l(l+1)}{r^2} \right) \right] r R_{l\omega}(r) = 0, \quad (1.7)$$

where $r \geq 2M$ is the function of r^* given by

$$r^* = r + 2M \ln(r/2M - 1), \quad 2M \leq r < \infty. \quad (1.8)$$

The ‘‘tortoise distance’’ r^* is the natural variable to use for a long-range potential.

The effective potential

$$V_{\text{eff}}(r^*, l) = V \left(\frac{r}{M}, l \right) = \left(1 - \frac{2M}{r} \right) \left(\frac{2M}{r^3} + \frac{l(l+1)}{r^2} \right) \quad (1.9)$$

is of finite range: it vanishes as $(r^*)^{-2}$ for $r^* \rightarrow \infty$ and as $\exp(r^*/2M)$ for $r^* \rightarrow -\infty$ (i.e., for $r - 2M \rightarrow 0^+$). (See Fig. 2 [13].)

Since black holes absorb waves of energy larger than V_{max} , black hole orbiting is different from the orbiting due to potentials with repulsive core considered by Ford and Wheeler. If the potential has a repulsive core, the angular momenta $l > \bar{l}$ and $l < \bar{l}$ will contribute to the orbiting cross section. If the potential does not have a repulsive core, only the angular momenta $l > \bar{l}$ will contribute to the orbiting cross section; the angular momenta $l < \bar{l}$ contribute to the absorption cross section.

C. Glory and orbiting cross sections computed by functional integrals

In this paper, using the same path integral techniques as in the derivation of glory scattering [6,9], we compute the dominating term $d\sigma_{\text{WKB}}^{\text{or}}$ in a semiclassical expansion of the cross section for orbiting scattering—first for particle scattering, then for wave scattering. We apply the result to the scattering of scalar waves by Schwarzschild black holes.

The functional integral used to compute the cross section of glory scattering and orbiting by black holes cannot be evaluated by any of the commonly used methods, discretization, analytical continuation, or WKB expan-

sions, for the following reasons.

(a) The paths take their values in Riemannian space, and discretization of the paths is ambiguous.

(b) Glory scattering and orbiting are scattering processes characterized by their initial and final momentum. This momentum-to-momentum transition cannot be computed from a position-to-position probability amplitude because there are no plane waves in curved spacetimes. Hence the path integral has to be set up for paths taking their values in phase space. Therefore, analytical continuation of a Wiener-type integral is not an option because there are no Wiener measurements for the space of paths in phase space (the positivity of the Jacobi operator in configuration space does not imply the positivity of the

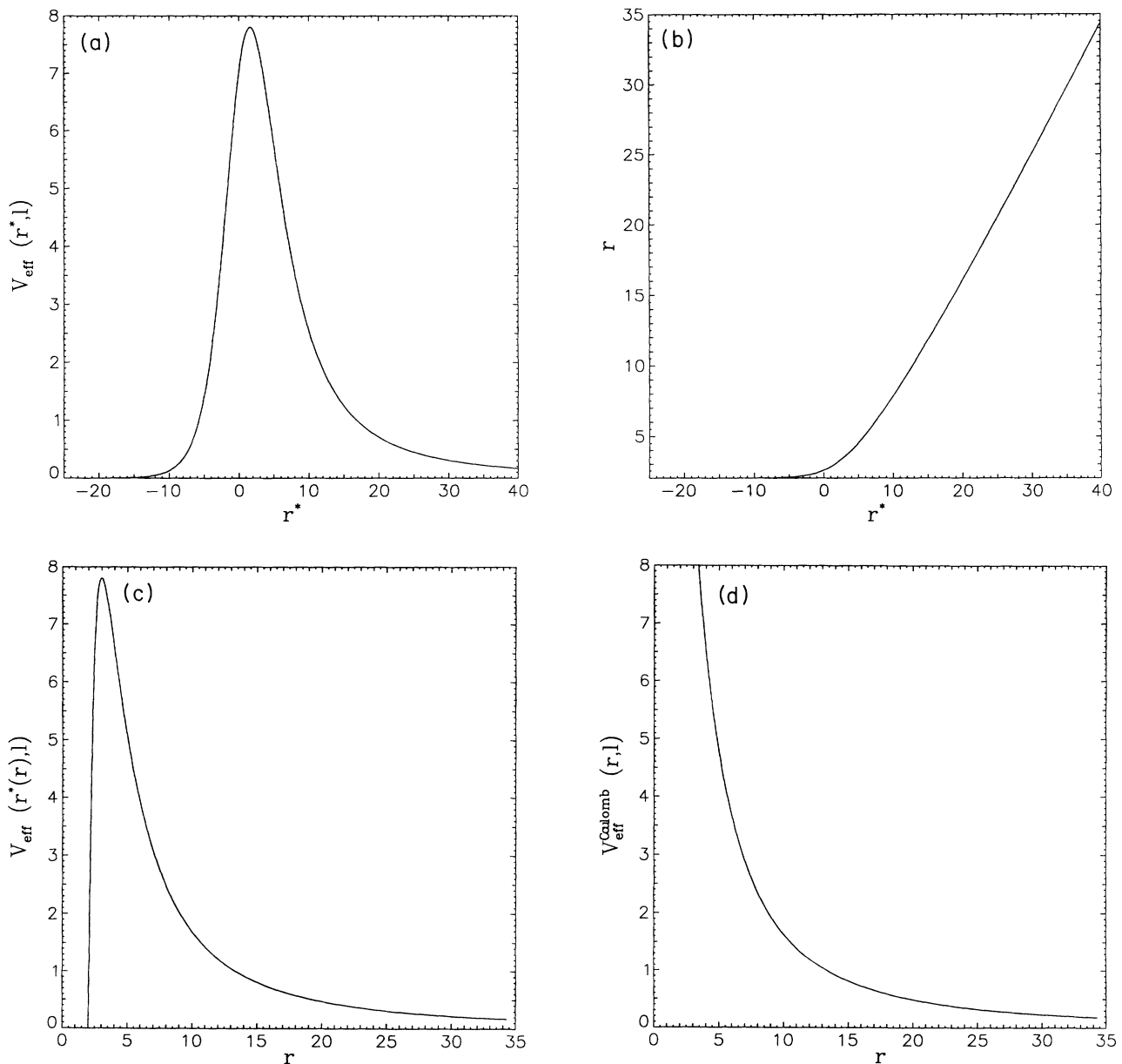


FIG. 2. $V_{\text{eff}}(r^*, l)$ increases like l^2 . The peak of $V_{\text{eff}}(r^*, l)$ at $r^* = r_{\text{max}}^*$ is responsible for the orbiting of particles with energy close to $V_{\text{eff}}(r_{\text{max}}^*, l)$. Here $l = 14$ and $M\omega = 2.5$. See Handler [13] for the Newton effective potential (d).

corresponding Jacobi operator in phase space).

(c) The critical points of the action are degenerate on several accounts. Hence the WKB approximation “breaks down,” and cannot be corrected heuristically.

On the other hand, the computational techniques [14–16] based on the definition of path integrals directly on the infinite-dimensional space of paths, proposed by DeWitt-Morette [17,18] and developed in collaboration with Nelson and Zhang, are suitable to compute glory and orbiting cross sections.

In Sec. II we derive the semiclassical approximation of the cross section. In Sec. III we compute the cross section numerically for several values of $M\omega$. The formula obtained in Sec. II gives an interpretation of the numerical cross sections. The numerical cross sections justify the approximations made in deriving the formula.

II. SEMICLASSICAL APPROXIMATION

A. Quantum-mechanical orbiting cross sections

The techniques developed for the path integral calculation of glory scattering [6] can be adapted for the calculation of orbiting cross sections, although the two phenomena differ on two accounts.

(a) Glories and rainbows occur when the critical points (classical solutions of the Euler-Lagrange equations) of the action functional are degenerate [6]. Orbiting, on the other hand, occurs when the deflection function is singular.

(b) Glories and rainbows occur near a definite observation angle. Orbiting contributes to all observation angles.

Quantum-mechanical scattering cross sections can be computed [19] in terms of the probability amplitude $K(\mathbf{p}_b, t_b; \mathbf{p}_a, t_a)$ that a particle known to have momentum \mathbf{p}_a at time t_a will be found with momentum \mathbf{p}_b at time t_b . We have previously computed [14] $K_{\text{WKB}}(\mathbf{p}_b, t_b; \mathbf{p}_a, t_a)$ when classical conservation laws limit the choice of the final momentum. Here we shall simply sketch a heuristic argument valid in flat spacetime for potentials with compact support; we refer the reader to [14] for a rigorous analysis of the general case:

$$K_{\text{WKB}}(\mathbf{p}_b, t_b; \mathbf{p}_a, t_a) = \text{spa} \int \exp[(i/\hbar)\mathbf{p}_a \cdot \mathbf{a}] K_{\text{WKB}}(\mathbf{p}_b, t_b; \mathbf{a}, t_a) d^3\mathbf{a}, \quad (2.1)$$

where spa stands for stationary phase approximation, and

$$K_{\text{WKB}}(\mathbf{p}_b, t_b; \mathbf{a}, t_a) = \left| \frac{\det \partial^2 S(\mathbf{p}_b, t_b; \mathbf{a}, t_a)}{\partial \mathbf{p}_b \partial \mathbf{a}} \right|^{1/2} \times \exp[(i/\hbar)S(\mathbf{p}_b, t_b; \mathbf{a}, t_a)]. \quad (2.2a)$$

Note that we use the same symbol K_{WKB} on both sides of Eq. (2.1). Hence, \mathbf{p}_a , \mathbf{a} , etc., in this and other equations are not treated as arguments of K_{WKB} but as labels which specify the probability amplitude.

The action function S is equal to the action functional evaluated along the classical path q with boundary condi-

tions indicated by the arguments of S :

$$S(\mathbf{p}_b, t_b; \mathbf{a}, t_a) = \int_{t_a}^{t_b} L(\mathbf{q}(t), \dot{\mathbf{q}}(t)) dt - \mathbf{p}_b \cdot \mathbf{q}(t_b), \quad (2.2b)$$

$$q(t_a) = \mathbf{a}, \quad \frac{\partial L}{\partial \dot{q}(t_b)} = \mathbf{p}_b.$$

In cylindrical coordinates $\mathbf{a} = (z, B, \varphi)$ with z along the direction of the incident wave and the scatterer at $z = 0$, B is the impact parameter, and φ the polar angle in the plane perpendicular to z ,

$$d^3\mathbf{a} = B dB dz d\varphi = |\mathbf{p}_a|^{-2} dl dz d\varphi,$$

where $l = B|\mathbf{p}_a|$ is the incoming angular momentum with respect to the scatterer. Provided one is far from glory scattering, the stationary phase φ integral determines a single critical value φ_0 corresponding to the plane of the classical path with boundary value \mathbf{a}, \mathbf{p}_b . The stationary phase z integral does not select a particular value z_0 but introduces $\delta(|\mathbf{p}_b| - |\mathbf{p}_a|)$, which reflects the energy conservation during the scattering process. Hence,²

$$K_{\text{WKB}}(\mathbf{p}_b, t_b; \mathbf{p}_a, t_a) = 2\pi\hbar\delta(|\mathbf{p}_b| - |\mathbf{p}_a|)|\mathbf{p}_a|^{-2} \times \text{spa} \int_0^\infty K_{\text{WKB}}(\mathbf{p}_b, t_b; l, \varphi_0, t_a) l dl. \quad (2.3)$$

When orbiting occurs, an infinite number of classical paths contribute³ to $K_{\text{WKB}}(\mathbf{p}_b; \mathbf{p}_a)$. We shall now examine this situation. Let θ be the observation angle, $\bar{\Theta}(l)$ be the rotation angle of a particle moving along a classical trajectory, and $\Theta(l)$ be the deflection function. For attractive potentials (see Fig. 3), $\bar{\Theta}$ is positive for negative impact parameters (trajectory deflected counterclockwise), and negative for positive impact parameters (trajectory deflected clockwise). On the other hand, the

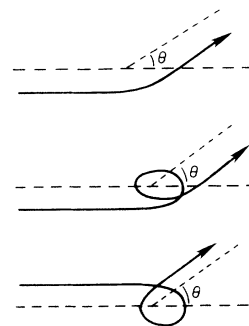


FIG. 3. The observation angle $0 \leq \theta < \pi$. The deflection function $\Theta(l)$ is negative for attractive potentials $\Theta(l) = -|\bar{\Theta}(l)|$, where $\bar{\Theta}(l)$ is the rotation angle of a particle moving along the classical trajectory.

²This is, with a change of notation, the same equation as (17) in Ref. [6]. See (2.57a) the explicit expression for $K_{\text{WKB}}(\mathbf{p}_b, t_b; l, \varphi_0, t_a)$.

³We omit the labels “ t_a, t_b ” when not necessary.

deflection function $\Theta(l) = \partial S(l)/\partial l$, where $S(l)$ is defined by (2.57), is insensitive to the orientation of the trajectory. Hence [see also 1,2] $\Theta(l) = -|\bar{\Theta}(l)|$ for attractive potentials.

The scattering angle $\theta(l)$ is the equivalence class $[\Theta(l)]$ where $\Theta(l) \simeq \Theta(l')$ if they yield the same scattering angle. For $l > \bar{l}$, the scattering angle $\theta(l)$ is plotted in Fig. 4.

If the boundary conditions $(\mathbf{p}_b, \mathbf{p}_a)$ define a finite number of classical paths “sufficiently distinct,”⁴ then we can write

$$K_{\text{WKB}}(\mathbf{p}_b; \mathbf{p}_a) = \sum_i K_{\text{WKB}}^i(\mathbf{p}_b; \mathbf{p}_a),$$

one term computed for each classical path. In our problem, there is only one path sufficiently distinct from the others, namely, the nonorbiting path:

$$K_{\text{WKB}}(\mathbf{p}_b; \mathbf{p}_a) = K(\text{nonorbiting}) + K(\text{orbiting}).$$

More precisely we shall split the domain of l integration in (2.3) into four domains:

Domain	Angular momentum	Scattering with repulsive core	Black-hole scattering
Δ_I	$0 \leq l' < l'_\pi$	No orbiting	Absorption
Δ_{II}	$l'_\pi \leq l' < \bar{l}$	Orbiting	Absorption
Δ_{III}	$\bar{l} \leq l < l_\pi$	Orbiting	Orbiting
Δ_{IV}	$l_\pi \leq l < \infty$	No orbiting	No orbiting

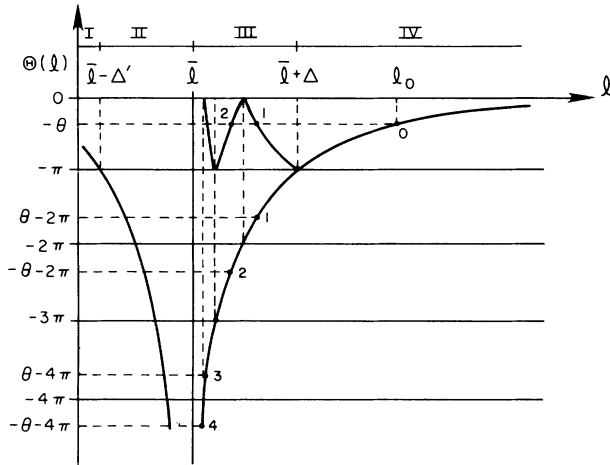


FIG. 4. Near \bar{l} , the deflection function $\Theta(l)$ is given by (2.4b). For large values of l (large impact parameters) $\Theta(l)$ tends to zero. The equivalence class $\theta(l) = [\Theta(l)]$ is plotted for $l > \bar{l}$. The points 1, 2, 3, and 4 are in the same equivalence class; the points 1 and 3 correspond to particles with different l which have orbited zero time, once, or twice counterclockwise; the points 2 and 4 correspond to particles with different l which have orbited once or twice clockwise. l is an infinite valued function of θ . For $l > \bar{l}$, let l_0 be the solution of $\Theta(l_0) = -\theta$ and for $l < \bar{l}$, let l'_0 be the solution of $\Theta(l'_0) = -\theta$.

⁴Classical paths close to coalescing (i.e., initial and final points of classical paths in phase space to conjugate points) are not “sufficiently distinct.”

Omitting the WKB label, we set

$$K = K^I + K^{II} + K^{III} + K^{IV} \\ = K^I(1 + K^{II}/K^I) + K^{IV}(1 + K^{III}/K^{IV}). \quad (2.4)$$

In the domains I and IV, l is a single-valued function of the observation angle θ ; K^I and K^{IV} can be computed by the standard stationary phase method.

For black hole scattering the only contribution to the orbiting cross section comes from $l > \bar{l}$:

$$K = K^{IV} \left[1 + \frac{K^{III}}{K^{IV}} \right].$$

In Ref. [6], we have derived the scattering cross section $d\sigma/d\Omega$ in terms of the momentum-to-momentum amplitude $K(\mathbf{p}_b; \mathbf{p}_a)$, normalized to be of dimension L^3 . When, as is the case here, the amplitude is of the form

$$K(\mathbf{p}_b; \mathbf{p}_a) = 2\pi\hbar\delta(|\mathbf{p}_b| - |\mathbf{p}_a|)\hat{K}(\mathbf{p}_b; \mathbf{p}_a), \quad (2.5)$$

which defines \hat{K} ; the cross section is

$$\frac{d\sigma}{d\Omega} = \frac{|p_a|^2}{(2\pi\hbar)^2} |\hat{K}(\mathbf{p}_b; \mathbf{p}_a)|^2 \quad \text{with} \quad |\mathbf{p}_b| = |\mathbf{p}_a|. \quad (2.6)$$

However, the normalization of the amplitude K is irrelevant in our calculation for the following reason. It follows from (2.15) that

$$\hat{K} = \hat{K}^{IV}(1 + \hat{K}^{III}/\hat{K}^{IV})$$

and

$$\frac{d\sigma}{d\Omega} = \frac{d\bar{\sigma}}{d\Omega} |1 + \hat{K}^{III}/\hat{K}^{IV}|^2. \quad (2.7)$$

For large impact parameter, the effective potential $V_{\text{eff}}(r^*, l)$ [Fig. 2(c)] is well approximated by a Newton effective potential [(Fig. 2(d))] and we shall replace $d\bar{\sigma}/d\Omega$ by the Rutherford cross section

$$\frac{d\bar{\sigma}}{d\Omega} \approx \frac{G^2 M^2}{c^4} \frac{1}{\sin^4 \theta/2}. \quad (2.8)$$

It is then not necessary to use the coefficient of proportionality between $d\sigma/d\Omega$ and $|\hat{K}|^2$ given by (2.6).

At first the approximation (2.8) was made to simplify the calculation and to isolate the orbiting effects $\hat{K}^{III}/\hat{K}^{IV}$. The numerical calculation, reported in Sec. III justifies this approximation.

The explicit calculation of K^{III}/K^{IV} for scalar waves orbiting Schwarzschild black holes is given in Sec. II C, after we prove in Sec. II B that $K(\mathbf{p}_b; \mathbf{p}_a)$ can be used for computing wave scattering. In this section, we give the generic properties of the orbiting contributions K^{II}/K^I or K^{III}/K^{IV} and a blueprint for computing the orbiting contributions, starting from (2.3).

It will be shown (2.57a) that

$$K(\mathbf{p}_b; l, \varphi_0) = A f(l) \exp \left[\frac{i}{\hbar} [S(l) + |\bar{\Theta}(l)|] \right], \quad (2.9)$$

where A is independent of l , $f(l)$ is a slowly varying function of l , $S(l)$ is the action function (2.57b), and $\bar{\Theta}$ is

the rotation angle at time t_b . The stationary phase approximation in (2.3) selects the values of l such that

$$\frac{d}{dl}[S(l) + |\bar{\Theta}|l] = 0, \tag{2.10a}$$

$$\frac{dS(l)}{dl} \equiv \Theta(l) = -|\bar{\Theta}|. \tag{2.10b}$$

There are an infinite number of values of l which satisfy this equation for a given value of θ —i.e., for a given value of \mathbf{p}_b ; since

$$\bar{\Theta}_n = \theta + 2n\pi, \quad \bar{\Theta}_m = \theta - 2m\pi \quad \text{with } m, n \geq 1, \tag{2.11}$$

any l_n or l_m such that

$$\Theta(l_n) = -|\bar{\Theta}_n| \quad \text{or} \quad \Theta(l_m) = -|\bar{\Theta}_m|$$

is an acceptable value of l contributing to $K(\mathbf{p}_b, \mathbf{p}_a)$. In classical mechanics, the boundary conditions $\{(l, \varphi_0), \mathbf{p}_b\}$ determine a unique path. In quantum mechanics, $K(\mathbf{p}_b; l, \varphi_0)$ is the sum over all paths with boundary conditions $\{(l, \varphi_0), \mathbf{p}_b\}$. These paths are in different homotopy classes and it has been shown [20] that the total amplitude $K(\mathbf{p}_b; l, \varphi_0)$ is a linear combination of the partial amplitudes $K^k(\mathbf{p}_b; l, \varphi_0)$ obtained by summing over all the paths in the k -homotopy class. The coefficients $\chi^\alpha(k)$ of this linear combination form a one-dimensional, unitary representation of the fundamental group $\pi_1(\mathbb{R}^2 - \{0\}) = \mathbb{Z}$:

$$K^\alpha = \sum_k \chi^\alpha(k) K^k = \sum_{k=-\infty}^{+\infty} e^{2\pi i \alpha k} K^k. \tag{2.12}$$

The different representations are labeled by $0 \leq \alpha < 1$. They define different propagators. Dowker [21] has shown that choosing α in Eq. (2.12) is equivalent to choosing the phase change of the multivalued wave function of the system,

$$\Psi(x) \rightarrow \exp(2\pi i \alpha k) \Psi(x),$$

after circling k times around the scatterer. There is no *a priori* reason for choosing $\alpha=0$ and the choice of different quantum representations corresponding to a given classical system is an important problem which has received only a few answers: e.g., boson and fermion representations of systems of indistinguishable particles, the existence of nonequivalent θ vacua in QCD, and the Schwinger model in two-dimensional QED [22].

In this paper we compute K_{WKB}^α explicitly for $\alpha=0$ for two reasons: it is simpler and it is the quantity needed to compute classical wave scattering where the solution is single valued. We shall simply omit the label α and indicate in Eq. (2.16) how the result is changed when $\alpha \neq 0$. Equation (2.12) can be written

$$K(\mathbf{p}_b; l, \varphi_0) = \sum_{m=1}^{\infty} K(|\bar{\Theta}_m|) + \sum_{n=1}^{\infty} K(|\bar{\Theta}_n|), \tag{2.13}$$

$l \in \Delta_{\text{II}}, \Delta_{\text{III}},$

where we have used $|\bar{\Theta}_m|$ and $|\bar{\Theta}_n|$ to label the homotopy classes. Given the form (2.9) of $K(\mathbf{p}_b; l, \varphi)$ and the values (2.11) of $\bar{\Theta}$, this equation gives

$$K(\mathbf{p}_b; l, \varphi_0) = Af(l) \exp\left[\frac{i}{\hbar} S(l)\right] \left\{ \sum_m \exp\left[\frac{i}{\hbar} l(-\theta + 2m\pi)\right] + \sum_n \exp\left[\frac{i}{\hbar} l(\theta + 2n\pi)\right] \right\} \tag{2.14}$$

$$= iAf(l) \exp\left[\frac{i}{\hbar} S(l)\right] \exp\left[\frac{i}{\hbar} \pi l\right] \cos\frac{\theta l}{\hbar} / \sin\frac{\pi l}{\hbar}. \tag{2.15}$$

With $\alpha \neq 0$ in Eq. (2.11), and $\hbar=1$, the term $\cos \theta l / \sin \pi l$ in the above equation is replaced by

$$\frac{1}{2} \frac{\exp[i(\theta l + \pi \alpha)]}{\sin \pi(l + \alpha)} + \frac{1}{2} \frac{\exp[-i(\theta l + \pi \alpha)]}{\sin \pi(l + \alpha)}. \tag{2.16}$$

We now insert $K(\mathbf{p}_b; l, \varphi_0)$ in (2.3) and integrate it in the small domains $\Delta_{\text{II,III}}$:

$$\int_{\Delta_{\text{II,III}}} K(\mathbf{p}_b; l, \varphi_0) l \, dl \simeq iAf(\bar{l}) I_1, \tag{2.17}$$

where we have assumed that $f(l)$ is a slowly varying function of l and

$$I_1 := \int_{\bar{l}}^{l_\pi} \exp\{i[S(l) + \pi l]/\hbar\} \frac{\cos \theta l / \hbar}{\sin \pi l / \hbar} l \, dl. \tag{2.18}$$

In conclusion

$$\frac{K^{\text{III}}}{K^{\text{IV}}} \simeq \frac{iAf(\bar{l}) I_1}{\text{spa} \int_{l_\pi}^{\infty} K(\bar{\mathbf{p}}_b; l, \varphi_0) l \, dl}, \tag{2.19}$$

In Sec. II C we compute explicitly $K^{\text{III}}/K^{\text{IV}}$. The calculation of $K^{\text{II}}/K^{\text{I}}$ is similar with l' replacing l , but with one important difference: K^{I} and K^{II} correspond to values of $l < \bar{l}$; i.e., they appear when the effective potential is of the type sketched on Fig. 5:

$$\Delta S = 2 \int_{r_1}^{r_2} p_r \, dr, \tag{2.20}$$

where p_r is the momentum conjugate to the radial variable, and r_1 and r_2 are the values of r indicated on Fig. 5.

The expansion of $S(l)$ near $S(l)$ is given by [2]

$$S(l) = S(\bar{l}) + a(l - \bar{l}) + b(l - \bar{l}) \ln(l/\bar{l} - 1) + O((l - \bar{l})^2), \quad l > \bar{l} \quad (2.21)$$

$$S(l) = S(\bar{l}) + \Delta S + c(l - \bar{l}) + 2b(l - \bar{l}) \ln(l - l/\bar{l}) + O((l - \bar{l})^2), \quad l < \bar{l}. \quad (2.22)$$

and

If we repeat the calculation carried out in Sec. II C for black-hole scattering, we obtain, when $l < \bar{l}$ contributes also to the cross section,

$$K_{\text{WKB}}(\mathbf{p}_b, t_b; \mathbf{p}_a, t_a) = K^I (1 + u(l'_0) \cos(\theta \bar{l} / \hbar)) \exp\{i/\hbar [S(\bar{l}) + \Delta S - S(l'_0) - \Theta \theta l'_0 + \pi \bar{l}]\} + K^{IV} (1 + u(l_0) \cos(\theta \bar{l} / \hbar)) \exp\{i/\hbar [S(\bar{l}) - S(l_0) - \theta l_0 + \pi \bar{l}]\}, \quad (2.23)$$

where

$$u(l_0) = i \frac{l_\pi - \bar{l}}{(2\pi\hbar)^{1/2}} \left[\sin \pi \frac{\bar{l}}{\hbar} \right]^{-1} \left[\frac{\partial^2 S}{\partial l_0^2} \right]^{1/2}.$$

B. Orbiting classical waves

Classical waves can be said to be orbiting if the characteristic system of their eikonal equation defines an orbiting flow—more precisely, a flow which includes some orbiting paths. It is then natural to investigate if the quantum-mechanical orbiting cross section (2.7) can be used for computing the classical wave orbiting cross section. We shall show that the answer is “yes, with proper modification”; more generally, we shall show how quantum-mechanical scattering calculations can be used in solving some classical wave scattering problems. For time-independent systems, the quantum-mechanical wave $\Psi(x, t) = \exp(i\omega t)\Psi(x)$ solution of a Schrödinger equation is, with minor modifications, a solution of a wave equation, but this is of limited use. For time-dependent systems, Zhang [23] has shown that classical wave scattering on an asymptotically flat manifold X (e.g., spacetime) can be obtained from solutions of a parabolic equation on $X \times \mathbb{R}$ of the “relativistic Schrödinger” type [Eqs. (2.29) and (2.30)]. Consider a wave operator $H(x, i\partial_\mu)$, with $x \in X^4 = M \times \mathbb{R}$ and $\partial_\mu = \partial/\partial x^\mu$, and a wave equation

$$[H(x, i\partial_\mu) - m^2]\phi_p(x) = 0, \quad x \in X^4, \quad (2.24a)$$

$$\lim_{x^0 \rightarrow -\infty} \phi_p(x) = f_p(x), \quad (2.24b)$$

where $f_p(x)$ is defined as follows. Let $\{f_p\}$ be a complete set of orthonormal functions on X ; i.e.,

$$\int_{\mathbb{R}^4} f_p(x) f_p^*(x') dp = \delta(x, x'), \quad p \in \mathbb{R}^4, \\ \int_X f_p(x) f_p^*(x) d\tau(x) = \delta(p, p').$$

If $X = \mathbb{R}^4$, we choose $\{f_p\}$ to be a set of plane waves; if X is a Schwarzschild manifold [Eq. (0.6)], we choose $\{f_p\}$ to be a set of distorted plane waves defined outside the black hole located at the origin by

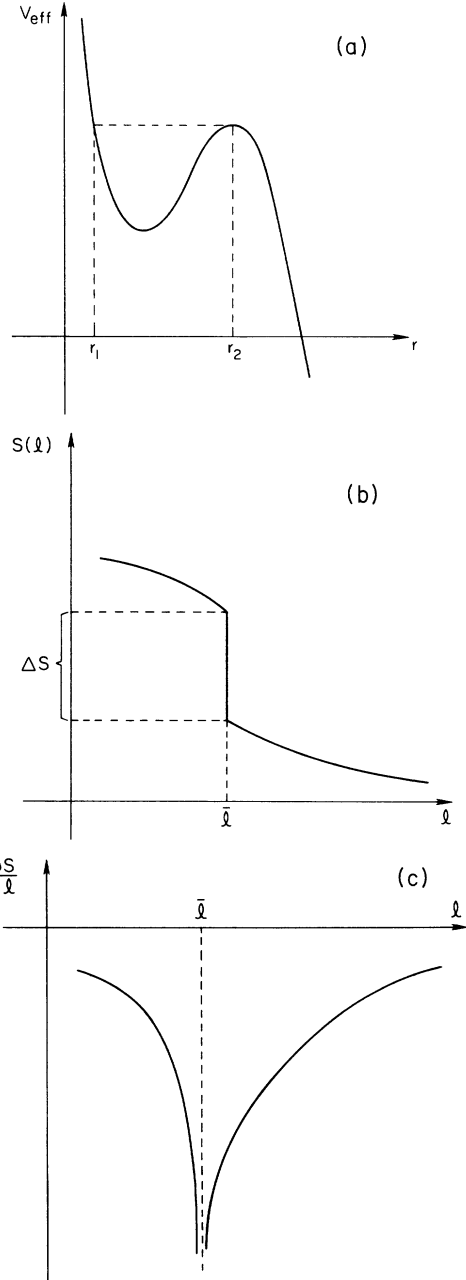


FIG. 5. The action function $S(l)$ and the deflection function $\Theta(l) = \partial S / \partial l$ are sketched for the case of an effective potential $V_{\text{eff}}(r)$ with repulsive core.

$$f_p(x) = \frac{r^*}{r(1-2M/r)^{1/2}} \exp(ipx^*) \equiv C(r) \exp(ipx^*), \quad (2.25)$$

with r^* the ‘‘tortoise distance’’ defined by

$$r^* = r + 2M \ln(r/2M - 1) \text{ for } 2M \leq r < \infty \quad (2.26)$$

$$x^* = (x^0, (r^*/r)\mathbf{x}), \quad px^* = p_\mu x^{*\mu},$$

$$p^2 = g^{\mu\nu} p_\mu p_\nu, \quad p_\mu = (p_0, \mathbf{p}).$$

The use of arrows over spatial variables is not to be con-

strued as space being flat. We define f_p to be equal to f_p when p is on the mass shell,

$$p^2 = m^2.$$

If f_p is a distorted plane wave,

$$f_p(x) = \exp(i\omega x^0) g_p(\mathbf{x}), \quad \omega = (p^2 + m^2)^{1/2}. \quad (2.27)$$

Note that the family $\{g_p\}$ is an orthogonal family of functions on M . Zhang [23] has shown that the solution of Eq. (2.24a) with boundary values Eq. (2.24b) can be written

$$\phi_p(x) = \omega \pi^{-1} \int_0^\infty dp_0 \lim_{\varepsilon=0} \left[\int_0^\infty K^+(x, s; p, 0) \exp(im^2 s - \varepsilon s) ds + \int_{-\infty}^0 K^-(x, 0; p, s) \exp(im^2 + \varepsilon s) ds \right], \quad (2.28)$$

with $p_\mu = (p_0, \mathbf{p})$ and where K^\pm are solutions of a system of equations associated with the wave equations [Eqs. (2.24)]:

$$i\partial_s K^+(x, s; p, 0) = H(x, i\partial_\mu) K^+(x, s; p, 0), \quad s \geq 0, \quad (2.29a)$$

$$\lim_{s=0} K^+(x, s; p, 0) = f_p(x) \quad (2.29b)$$

and

$$i\partial_s K^-(x, 0; p, s) = H(x, i\partial_\mu) K^-(x, 0; p, s), \quad s \leq 0, \quad (2.30a)$$

$$\lim_{s=0} K^-(x, 0; p, s) = f_p(x), \quad (2.30b)$$

where $\partial_s = \partial/\partial s$.

A path integral solution of Eqs. (2.29) or (2.30) is a sum over all ‘‘relativistic’’ paths,

$$\mathbf{x}: \mathbb{R} \rightarrow M \text{ by } s \mapsto \mathbf{x}(s),$$

with the boundary conditions for Eq. (2.29)

$$\mathbf{x}(s) = \mathbf{x}, \quad \mathbf{p}(0) = \mathbf{p},$$

and for Eq. (2.30)

$$\mathbf{x}(0) = \mathbf{x}, \quad \mathbf{p}(s) = \mathbf{p},$$

where $\mathbf{p}(s) = \partial L / \partial \dot{\mathbf{x}}(s)$.

We recall that the relativistic propagator K^+ has extensively been used [24] since it was introduced [25,26] in 1950 for the construction of the Feynman Green’s function which propagates positive frequencies in the future and negative frequencies in the past.

The ‘‘fifth’’ parameter s , also, but erroneously, called ‘‘proper time’’, is conjugate to m^2 in the sense that $K^\pm(s)$ propagates particles of all masses and its Fourier transform at m^2 ‘‘selects the mass mode m .’’ One selects the zero mass mode for massless waves.

We shall carry out explicitly the calculation of the high-frequency approximation ϕ_{WKB} of ϕ given by Eq. (2.28) and of the high-frequency approximation of the S-matrix element $\langle \mathbf{p}' | S | \mathbf{p} \rangle$, which is defined by

$$\langle \mathbf{p}' | S | \mathbf{p} \rangle = (f_{\mathbf{p}'}, \phi_{\mathbf{p}}) \equiv \int_M f_{\mathbf{p}'}^*(x) \phi_{\mathbf{p}}(x) d\tau(\mathbf{x}), \quad (2.31)$$

where f_p is the on-shell value of an element of the orthonormal set $\{f_p\}$. In order to identify the various high-frequency approximations, we scale s and x ; set

$$s = v\bar{s}, \quad x = v\bar{x}$$

and define

$$\bar{K}(\bar{x}, \bar{s}) = K(x(\bar{x}), s(\bar{s})),$$

$$\bar{H}(\bar{x}, i\nu^{-1}\partial_{\bar{\mu}}) = H(x(\bar{x}), i\partial/\partial x^\mu(\bar{x})).$$

\bar{K}^\pm is a solution of

$$i\nu^{-1}\partial_{\bar{s}} \bar{K}^\pm = \bar{H}(\bar{x}, i\nu^{-1}\partial_{\bar{\mu}}) \bar{K}^\pm;$$

its WKB approximation is the leading term of its expansion in powers of ν^{-1} , and ϕ_{WKB} is the stationary phase approximation of Eq. (2.28) with the integrands replaced by their WKB approximations. We have previously [17,18] computed the WKB approximation

$$K_{\text{WKB}}(\beta, t_b; \alpha, t_a) = C(\beta, \alpha) |\det_{\mu, \nu} \partial^2 S(\beta, t_b; \alpha, t_a) / \partial \beta^\nu \partial \alpha^\nu|^{1/2} \times \exp[i\nu S(p, t_b; \alpha, t_a)] \quad (2.32)$$

for propagators K on Riemannian manifolds M^n arbitrary dimensions n with arbitrary initial and final conditions (β, α) . For K^+ , $\beta = \bar{x}$, $\alpha = p$, $t_b = \bar{s}$, $t_a = 0$,

$$C(\beta, \alpha) = (2\pi\nu^{-1})^{-n/2}.$$

$\bar{S}(\bar{x}, \bar{s}; p, 0)$ is the classical action function, i.e., the action functional, corresponding to a classical Hamiltonian $\bar{H}(\bar{x}, p)$, evaluated along a classical solution \bar{x} with boundary conditions $\bar{x}(\bar{s}) = \bar{x}$, $\mathbf{p}(0) = p$. Hence

$$\frac{\partial \bar{S}}{\partial \bar{s}} = -\bar{H},$$

and, since \bar{H} is independent of s ,

$$\bar{S}(\bar{x}, \bar{s}; p, 0) = -\bar{H}(\bar{x}, p)\bar{s} + \bar{S}_0(\bar{x}, p). \quad (2.33)$$

For a scalar wave [Eq. (2.27)],

$$\bar{H}(\bar{x}, p) = g^{\mu\nu}(\nu\bar{x})p_\mu p_\nu. \quad (2.34)$$

At $\bar{x}(s = \pm\infty)$, the space X has been assumed flat

$$g^{\mu\nu}[\nu\bar{x}(s = \pm\infty)] = \eta^{\mu\nu}.$$

In the relativistic classical motion $\bar{x}(s)$ parametrized by s , the relativistic Hamiltonian is independent of s ; hence,

$$\bar{H}(\bar{x}, p) = \eta^{\mu\nu}p_\mu p_\nu, \quad (2.35)$$

so

$$\frac{\partial^2 \bar{S}(\bar{x}, \bar{s}; p, 0)}{\partial \bar{x}^\mu \partial p_\nu} = \frac{\partial^2 \bar{S}_0(\bar{x}, p)}{\partial \bar{x}^\mu \partial p_\nu}. \quad (2.36)$$

Hence inserting Eqs. (2.31), (2.33), and (2.34) into Eq. (2.30), we have, for $s \leq 0$,

$$K_{\text{WKB}}^-(x, 0; p, s) = (2\pi\nu^{-1})^{-n/2} \det_{\mu\nu} \left| \frac{\partial^2 \bar{S}_0(\bar{x}, p)}{\partial \bar{x}^\mu \partial p_\nu} \right|^{1/2} \times \exp\{i\nu[\bar{S}_0(\bar{x}, p) - p^2 \bar{s}]\} \quad (2.37a)$$

and, for $s \geq 0$,

$$K_{\text{WKB}}^+(x, s; p, 0) = (2\pi\nu^{-1})^{-n/2} \det_{\mu\nu} \left| \frac{\partial^2 \bar{S}_0(\bar{x}, p)}{\partial \bar{x}^\mu \partial p_\nu} \right|^{1/2} \times \exp\{i\nu[\bar{S}_0(\bar{x}, p) - p^2 \bar{s}]\}, \quad (2.37b)$$

so

$$K_{\text{WKB}}^+(x, 0; p, 0) = K_{\text{WKB}}^-(x, 0; p, 0)$$

and we define a continuous function K_{WKB} of s by

$$K_{\text{WKB}}(x, s; p, 0) = \begin{cases} K_{\text{WKB}}^+(x, s; p, 0) & \text{for } s \geq 0, \\ K_{\text{WKB}}^-(x, 0; p, s) & \text{for } s \leq 0. \end{cases} \quad (2.38)$$

Equation (2.5) becomes

$$\phi_{\mathbf{p}}^{\text{WKB}}(x) = \omega\pi^{-1} \int_0^\infty dp_0 \lim_{\epsilon=0} \int_{-\infty}^{+\infty} K_{\text{WKB}}(x, s; p, 0) \times \exp(im^2 s - \epsilon|s|) ds. \quad (2.39)$$

The s dependence of K_{WKB} can be read from Eqs. (2.37) and the s integral yields

$$\lim_{\epsilon=0} \int_{-\infty}^{+\infty} ds \exp(im^2 s - \epsilon|s|) \exp(ip^2 s) = 2\pi\delta(m^2 - p^2) = 2\pi\delta(p_0^2 - \omega^2); \quad (2.40)$$

it follows from Eq. (2.31) and from $x = \nu\bar{x}$ that

$$\langle \mathbf{p}' | \mathbf{S} | \mathbf{p} \rangle_{\text{WKB}} = \text{spa} \int_M d\tau(\mathbf{x}) f_{\mathbf{p}'}^*(x) (\nu/2\pi)^{n/2} \left| \det_{\mu\nu} \frac{\partial^2 S_0(x, p)}{\partial x^\mu \partial p_\nu} \right|^{1/2} \exp[i\nu S_0(x, p)] \quad \text{for } p^2 = m^2 \quad (2.41)$$

$$= \text{spa} \int_M d\tau(\mathbf{x}) f_{\mathbf{p}'}^*(x) K_{\text{WKB}}(x, \mathbf{p}), \quad (2.42)$$

where

$$K_{\text{WKB}}(x, \mathbf{p}) = (\nu/2\pi)^{n/2} \left| \det_{\mu\nu} \frac{\partial^2 S_0(x, p)}{\partial x^\mu \partial p_\nu} \right|^{1/2} \exp[i\nu S_0(x, p)] \quad \text{for } p^2 = m^2.$$

First we note that the right-hand side of Eq. (2.41) is independent of x^0 , as it should be. Indeed, when $p^2 = m^2$ the dependence of $\exp[i\nu S_0(x, p)]$ on x^0 precisely cancels the dependence of $f_{\mathbf{p}'}^*(x)$ on x^0 , and the determinant does not depend on x^0 . The stationary phase approximation of integrals such as Eq. (2.42) has been analyzed in [14]. It has been shown that if the flows associated with $f_{\mathbf{p}'}^*(x)$ and by $K_{\text{WKB}}(x, \mathbf{p})$ have no common trajectory, then the integral is of order ν^{-N} for arbitrary N , i.e., the integral vanishes. If the flows have one common trajectory,

$$\langle \mathbf{p}' | \mathbf{S} | \mathbf{p} \rangle = K_{\text{WKB}}(\mathbf{p}', \mathbf{p}) \equiv (2\pi\nu^{-1}) \delta(|\mathbf{p}'| - |\mathbf{p}|) \hat{K}(\mathbf{p}', \mathbf{p}). \quad (2.43)$$

WKB scattering of waves can be computed in terms of the particle propagator $K_{\text{WKB}}(\mathbf{p}', \mathbf{p})$ because the characteristic system of the WKB approximation of the wave

equation (eikonal equation) defines a flow. This flow can be used in the WKB approximation of a “relativistic” path integral (paths in \mathbb{R}^4 , Lorentzian metric) parametrized by a fifth parameter.

C. Scalar waves orbiting Schwarzschild black holes

In order to compute the cross section for the scattering of scalar waves by Schwarzschild black holes, we need, according to the discussion in paragraph 3, to compute

$$K_{\text{WKB}}(\mathbf{p}_b, t_b; \mathbf{p}_a, t_a) \equiv K(\mathbf{p}_b \cdot \mathbf{p}_a),$$

and according to the discussion in paragraph 1, we need to express $K(\mathbf{p}_b; \mathbf{p}_a)$ in terms of

$$\int_0^\infty K_{\text{WKB}}(\mathbf{p}_b; l, \varphi_0) l dl$$

as per (2.3). Following the blueprint outlined in paragraph 1, we insert (2.2a) and (2.1b) into (2.1) we obtain

$$K(\mathbf{p}_b; \mathbf{p}_a) = \int \left| \det \frac{\partial^2 S}{\partial p_b \partial a} \right|^{1/2} \exp \left[\frac{i}{\hbar} \mathbf{p}_a \cdot \mathbf{a} + \frac{i}{\hbar} S \right] d\mathbf{a}, \tag{2.44}$$

where the action function is a function of \mathbf{a} and \mathbf{p}_b ,

$$S(\mathbf{p}_b; \mathbf{a}) = \int_{t_a}^{t_b} L dt - \mathbf{p}_b \cdot \mathbf{q}(t_b) \\ = \int_{t_a}^{t_b} \mathbf{p} \cdot d\mathbf{q} - E(t_b - t_a) - \mathbf{p}_b \cdot \mathbf{q}(t_b), \tag{2.45}$$

the Lagrangian being computed along the classical path \mathbf{q} with initial position \mathbf{a} , final momentum \mathbf{p}_b . We shall use cylindrical coordinates

$$\mathbf{a} = (z, B, \varphi), \quad d^3\mathbf{a} = |\mathbf{p}_a|^{-2} l dl dz d\varphi$$

with the impact parameter $B = l/|\mathbf{p}_a|$, z along the direction of the incident wave, and the scatterer at $z = 0$. We write, using the arguments as labels and not as variables,

$$S(\mathbf{p}_b; \mathbf{a}) \equiv S[z, |\bar{\Theta}(l)|, \varphi]. \tag{2.46}$$

(i) The φ integration is performed by the stationary phase method which selects the value of φ , say φ_0 , determined by the boundary conditions $(\mathbf{a}, \mathbf{p}_b)$. The stationary phase approximation of the φ integration follows from

$$\int f(\varphi) \exp \left[\frac{i}{\hbar} S(\varphi) \right] d\varphi \\ \simeq (2\pi\hbar)^{1/2} \exp \left[\frac{i\pi}{4} \right] \left[\frac{\partial^2 S}{\partial \varphi_0^2} \right]^{-1/2} \\ \times f(\varphi_0) \exp \left[\frac{i}{\hbar} S(\varphi_0) \right],$$

giving

$$K(\mathbf{p}_b; \mathbf{p}_a) = 2\pi\hbar \delta(|\mathbf{p}_b| - |\mathbf{p}_a|) \exp(i\pi/4) \frac{1}{|\mathbf{p}_a|^2} \int_{\bar{l}}^{\infty} |\det S''|^{1/2} \left| \frac{\partial^2 S}{\partial \varphi_0^2} \right|^{-1/2} (2\pi\hbar)^{1/2} \\ \times \exp \left[\frac{i}{\hbar} \left(-E(t_b - t_a) + l(|\bar{\Theta}_b| + \pi) + 2 \int_{r_0}^{\infty} (p_r - |p_r|_{\infty}) dr \right) \right] l dl. \tag{2.52}$$

Remark. Strictly speaking $0 \leq l \leq \infty$ and not $\bar{l} \leq l < \infty$. Numerical integration has shown that the contributions of l to $K(\mathbf{p}_b; \mathbf{p}_a)$ in the absorption range $(0, \bar{l})$ can be neglected. This reflects the fact that, for each value of the observation angle θ , there is an infinite number of values of $l \in [\bar{l}, l_0]$ which contribute to the cross section.

(iii) Before performing the l integration, we compute $2 \int_{r_0}^{\infty} (p_r - |p_r|_{\infty}) dr$ for a Schwarzschild black hole. Set $p_{r*} dr^* = p_r dr$ where r^* is the tortoise distance defined

$$K(\mathbf{p}_b; \mathbf{p}_a) \\ = \frac{\exp(i\pi/4)}{|\mathbf{p}_a|^2} \int |\det S''|^{1/2} \left| \frac{\partial^2 S}{\partial \varphi_0^2} \right|^{-1/2} \sqrt{2\pi\hbar} \\ \times \exp \left[\frac{i}{\hbar} [|\mathbf{p}_a|z + S(z, |\bar{\Theta}(l)|, \varphi_0)] \right] \\ \times l dl dz, \tag{2.47}$$

S'' being the matrix $\partial^2 S / \partial p_b^\alpha \partial a^\beta$.

(ii) To perform the z integration we need to compute $S[z, |\bar{\Theta}(l)|, \varphi_0]$, i.e.,

$$S = \int_{t_a}^{t_b} L dt - \mathbf{p}_b \cdot \mathbf{q}(t_b) \\ = \int_{t_a}^{t_b} \mathbf{p} \cdot d\mathbf{q} - E(t_b - t_a) - \mathbf{p}_b \cdot \mathbf{q}(t_b). \tag{2.48}$$

In the φ_0 plane of the orbit $\mathbf{p} \cdot d\mathbf{q} = p_r dr + p_\theta d\theta$; with $\theta_a = -\pi$ we have

$$\int \mathbf{p} \cdot d\mathbf{q} - \mathbf{p}_b \cdot \mathbf{q}(t_b) = l(|\bar{\Theta}_b| + \pi) + \int_{t_a}^{t_b} p_r dr - \mathbf{p}_b \cdot \mathbf{q}(t_b) \tag{2.49}$$

having used the spherical symmetry of the scatterer which implies $p_\theta = \text{const} = l$. It remains to compute

$$\int_{t_a}^{t_b} p_r dr - \mathbf{p}_b \cdot \mathbf{q}(t_b) = 2 \int_{r_0}^{\infty} (p_r - |p_r|_{\infty}) dr - |\mathbf{p}_b|z, \tag{2.50}$$

where r_0 is the turning point of the radial coordinate, and where we have used

$$\int_{t_a}^{t_b} |p_r|_{\infty} dr - \mathbf{p}_b \cdot \mathbf{q}(t_b) = -|\mathbf{p}_b|z, \tag{2.51}$$

which follows from $|p_r|_{\infty} = \text{const} = |\mathbf{p}_b|$, and $|\mathbf{q}(t_a)| = z$.

Inserting S , as computed above, in (2.47) and performing the z integration we get

by Eq. (1.8):

$$\int_{r_0}^{\infty} (p_r - |p_r|_{\infty}) dr = \int_{r_0}^{\infty} (p_{r*} - |p_{r*}|_{\infty}) dr^*. \tag{2.53}$$

In terms of r^* the radial wave equation reads [11]

$$\left[\frac{d^2}{dr^{*2}} + \omega^2 - V_{\text{eff}}(r^*, l) \right] \exp \left[\frac{i}{\hbar} p_{r*} r^* \right] = 0 \tag{2.54}$$

with $V_{\text{eff}}(r^*, l)$ given by Eq. (1.9). We can read off p_{r*}

from Eq. (2.54) and use Eq. (1.8) to compute $dr^* = dr(1 - 2M/r)^{-1}$. Finally,

$$\begin{aligned} & \int_{r_0}^{\infty} (p_r - |p_r|_{\infty}) dr \\ &= \hbar \int_{v_0}^{\infty} \frac{1}{1 - 2/v} \{ [(M\omega)^2 - U(v, l)]^{1/2} - M\omega \} dv, \end{aligned} \quad (2.55)$$

where $v = r/M$, r is the Schwarzschild radial coordinate, and M is the mass of black hole, $v_0 = r_0/M$, r_0 the turning point of the radial coordinate, and

$$\begin{aligned} U(v, l) &= \left[1 - \frac{2}{v} \right] \left[\frac{2}{v^3} + \frac{l(l+1)}{v^2} \right] \\ &= M^2 V_{\text{eff}}(r^*, l). \end{aligned} \quad (2.56)$$

Inserting (2.55) into (2.52) gives

$$\begin{aligned} K(\mathbf{p}_b; \mathbf{p}_a) &= (2\pi\hbar) \delta(|\mathbf{p}_b| - |\mathbf{p}_a|) \exp(i\pi/4) \frac{1}{|\mathbf{p}_a|^2} \exp \left[-\frac{i}{\hbar} E(t_b - t_a) \right] \\ &\quad \times \int_{\bar{l}}^{\infty} |\det S''|^{1/2} \left| \frac{\partial^2 S}{\partial \varphi_0^2} \right|^{-1/2} (2\pi\hbar)^{1/2} \exp \left[\frac{i}{\hbar} [l|\bar{\Theta}_b| + S(l)] \right] l dl, \end{aligned} \quad (2.57a)$$

where

$$S(l) = \pi l + 2\hbar \int_{v_0}^{\infty} \frac{1}{1 - 2/v} \{ [(M\omega)^2 - U(v, l)]^{1/2} - M\omega \} dv. \quad (2.57b)$$

The angular momentum \bar{l} at which orbiting scattering occurs is determined by the equation

$$(M\omega)^2 - U(v_m(\bar{l}), \bar{l}) = 0, \quad (2.58)$$

where $v_m(l)$ is the value of $v = r/M$ at which the effective potential has its maximum. From the equation

$$\left. \frac{\partial U(v, l)}{\partial v} \right|_{v=v_m(l)} = 0, \quad (2.59)$$

it is easy to get $v_m(l) = 3$, and then the solution of Eq. (2.58) is $\bar{l} = 3\sqrt{3}M\omega$.

Equation (2.57a) gives K in the form (2.3) with $K(\mathbf{p}_b; l, \varphi_0)$ in the form (2.9):

$$\begin{aligned} K(\mathbf{p}_b; l, \varphi_0) &= Af(l) \exp \left[\frac{i}{\hbar} [S(l) + |\bar{\Theta}_b| l] \right] \\ &\quad \text{for } l \in \Delta_{I, IV} \end{aligned}$$

where

$$A = \exp(i\pi/4) (2\pi\hbar)^{1/2} \exp[-(i/\hbar)E(t_b - t_a)],$$

$$f(l) = |\det S''|^{1/2} \left| \frac{\partial^2 S}{\partial \varphi_0^2} \right|^{-1/2}.$$

According to the argument developed in Sec. II A, Eq. (2.19),

$$\frac{K^{\text{III}}}{K^{\text{IV}}} \simeq \frac{iAf(\bar{l})I_1}{\text{spa} \int_{l_{\pi}}^{\infty} K(\bar{\mathbf{p}}_b; l, \varphi_0) l dl},$$

where I_1 is defined by (2.18). The denominator is given by

$$\begin{aligned} & A_{\text{SP}} \int_{l_{\pi}}^{\infty} A |\det S''|^{1/2} \left| \frac{\partial^2 S}{\partial \varphi_0^2} \right|^{-1/2} \exp \left[\frac{i}{\hbar} [S(l) + |\bar{\Theta}_b| l] \right] l dl \\ &\equiv A_{\text{SP}} \int_{l_{\pi}}^{\infty} Af(l) \exp \left[\frac{i}{\hbar} [S(l) + |\bar{\Theta}_b| l] \right] l dl \\ &= (2\pi\hbar)^{1/2} \exp(i\pi/4) \left| \frac{d^2 S}{dl^2} \right|^{-1/2} Af(l_0) \exp \left[\frac{i}{\hbar} [S(l_0) + \theta l_0] \right] l_0, \end{aligned} \quad (2.60)$$

where l_0 is the angular momentum such that $dS/dl_0 = -\theta$, and⁵ $d^2S/dl_0^2 > 0$. It follows that

$$\frac{K^{\text{III}}}{K^{\text{IV}}} = i \frac{f(\bar{l})}{f(l_0)} \frac{1}{l_0 \sqrt{2\pi\hbar}} \left| \frac{d^2S}{dl_0^2} \right|^{1/2} \times \exp \left[-\frac{i}{\hbar} \left[S(l_0) + \theta l_0 + \frac{\pi}{4} \right] \right] I_1. \quad (2.61)$$

Hence [(2.7) and (2.8)],

$$\frac{d\sigma}{d\Omega} = \frac{d\bar{\sigma}}{d\Omega} \left| 1 + i \frac{f(\bar{l})}{f(l_0)} \frac{1}{l_0 \sqrt{2\pi\hbar}} \left| \frac{d^2S}{dl_0^2} \right|^{1/2} \times \exp \left[-\frac{i}{\hbar} [S(l_0) + \theta l_0 + \pi/4] \right] I_1 \right|^2. \quad (2.62)$$

For a Schwarzschild black hole,⁶ with $\hbar=1$, $G=1$, $c=1$, and using the Ford and Wheeler approximation (2.21) and $l(\theta)$ computed by Darwin (0.2) we obtain

$$\begin{aligned} \bar{l} &= 3\sqrt{3}M\omega, \\ l_0 = l(\theta) &= \bar{l} + 3.48 \exp(-\theta)M\omega, \\ l_\pi - \bar{l} &= 3.48 \exp(-\pi)M\omega = 0.15M\omega, \end{aligned} \quad (2.63)$$

$$S(l) = S(\bar{l}) + a(l - \bar{l}) + b(l - \bar{l}) \ln \left[\frac{l - \bar{l}}{\bar{l}} \right] \quad \text{for } l > \bar{l},$$

$$\Theta(l) = \frac{dS}{dl} = a + b + b \ln \left[\frac{l - \bar{l}}{\bar{l}} \right],$$

where a and b can be obtained by inverting (2.63):

$$\begin{aligned} \Theta(l) = -\theta &= -\ln(3.48M\omega/\bar{l}) + \ln \left[\frac{l - \bar{l}}{\bar{l}} \right] \\ &\Rightarrow b = 1, \quad a + b = -\ln(3.48M\omega/\bar{l}), \\ S(\bar{l}) - S(l) &= (\theta + 1)(l - \bar{l}), \\ S(\bar{l}) - S(l) + \pi\bar{l} - \theta l &= l - \bar{l} + (\pi - \theta)\bar{l}, \\ \frac{d^2S}{dl^2} &= (l - \bar{l})^{-1}. \end{aligned} \quad (2.64)$$

An approximation to the integral I_1 can be obtained by using the Darwin form for $S(l)$ so that

$$\begin{aligned} I_1 \simeq e^{iS(\bar{l})} \int_{\bar{l}}^{l_\pi} \exp \left\{ i \left[a(l - \bar{l}) + b(l - \bar{l}) \ln \left[\frac{l - \bar{l}}{\bar{l}} \right] \right. \right. \\ \left. \left. + \pi l \right] / \hbar \right\} \frac{\cos \theta l / \hbar}{\sin \pi l / \hbar} l \, dl \end{aligned} \quad (2.65)$$

and then assuming that the variations generated by all arguments are negligible relative to the πl terms. Thus the effect of the first two terms in the exponential can be accounted for by an overall phase shift and that $\cos \theta l / \hbar$ can be approximated by $\cos \theta \bar{l} / \hbar$. The integral (2.65) can now be written as

$$\begin{aligned} I_1 &\simeq \exp \{ i[S(\bar{l}) + \Phi] \} \bar{l} \cos(\theta \bar{l} / \hbar) \int_{\bar{l}}^{l_\pi} \frac{\exp(i\pi l / \hbar)}{\sin \pi l / \hbar} dl \\ &= \exp \{ i[S(\bar{l}) + \Phi] \} \bar{l} \cos(\theta \bar{l} / \hbar) \left[\frac{1}{\pi} \ln \frac{\sin |\pi(l_\pi - n)|}{\sin |\pi(\bar{l} - n)|} + i(l_\pi - \bar{l}) \right], \end{aligned} \quad (2.66)$$

where n is chosen such that $l_\pi - n < 1$ and $\bar{l} - n < 1$. The cross section (2.62) for scattering of scalar waves by Schwarzschild black holes can then be written as

$$\frac{d\sigma}{d\Omega} = \frac{d\bar{\sigma}}{d\Omega} \left| 1 + \frac{i}{\alpha} \frac{f(\bar{l})}{f(l_0)} \exp(i\beta) I_2 \right|^2 \quad (2.67)$$

where

$$\begin{aligned} \beta &= S(\bar{l}) - S(l_0) - \theta l_0 - \pi/4 + \Phi = [3.48 \exp(-\theta) - 3\sqrt{3}\theta]M\omega - \pi/4 + \Phi, \\ \alpha &= l_0 \sqrt{2\pi\hbar} \left| \frac{d^2S}{dl_0^2} \right|^{-1/2} = [3\sqrt{3} + 3.48 \exp(-\theta)]M\omega \sqrt{2\pi[3.48 \exp(-\theta)]M\omega}, \\ I_2 &= \cos \theta \bar{l} \left[\frac{\bar{l}}{\pi} \ln \frac{\sin |\pi(l_\pi - n)|}{\sin |\pi(\bar{l} - n)|} + i\bar{l}(l_\pi - \bar{l}) \right]. \end{aligned} \quad (2.68)$$

⁵See for instance in [27], p. 593, the reason for the factor $\exp(i\pi/4)$.

⁶With $\hbar \neq 1$, $G \neq 1$, $c \neq 1$, the first equation becomes $\bar{l}/\hbar = GM\omega/c^3$.

Before comparing this cross section with the numerical cross section computed in Sec. III, we shall recapitulate the approximations made in its derivation: WKB approximation; normalizing by the Rutherford cross section; ignoring $f(\bar{l})/f(l_0)$; simplifying phase variations of $S(l) - S(\bar{l})$ in (2.65).

None of these approximations affect the periodicity of the oscillations of the cross section due to orbiting—and this is our main concern in diagnosing the oscillations observed in the numerical cross sections. We anticipate the last two items will manifest themselves as discrepancies in the overall amplitude and phase of the oscillations because the analytic solution (2.67) has effectively two free parameters [$f(I)/f(l_0)$ and Φ] that will be chosen to fit the numerical results. How much they affect the oscillations can be assessed by comparison with the numerical calculations.

III. NUMERICAL CROSS SECTIONS

A. Method of partial waves

In Sec. III, we present the techniques used numerically to compute cross sections for the scattering of massless scalar (spin-0) waves in the static field of a Schwarzschild black hole. The method of partial waves is employed and solutions are separated into “plane” and “scattered” (spherical) waves of definite angular momentum. The phases of the scattered partial waves are determined numerically and used to compute the scattering cross section. Because we solve the exact differential wave equation, our results represent solutions over the full range of scattering and wave frequencies.

The equation governing massless scalar wave propagation is the wave equation [10,12]

$$\phi_{;\mu}^{\mu} = (-g)^{-1/2} \frac{\partial}{\partial x^{\mu}} \left[(-g)^{1/2} g^{\mu\nu} \frac{\partial}{\partial x^{\nu}} \phi \right] = 0, \quad (3.1)$$

where g is the determinant of the Schwarzschild metric tensor $g_{\mu\nu}$ defined by the line element

$$ds^2 = - \left[1 - \frac{2M}{r} \right] dt^2 + \frac{dr^2}{1 - 2M/r} + r^2 d\theta^2 + r^2 \sin^2\theta d\phi^2, \quad (3.2)$$

and M is the mass of the scatterer. The static and spherically symmetric nature of the metric (3.2) allows a natural separation of variables [10,12],

$$\phi = e^{-i\omega t} R_{l\omega}(r) Y_{lm}(\theta, \phi), \quad (3.3)$$

where $Y_{lm}(\theta, \phi)$ is a spherical harmonic and $R_{l\omega}(r)$ obeys the radial equation

$$\left[\frac{d^2}{dr^{*2}} + \omega^2 - V_{\text{eff}}(r^*, l) \right] r R_{l\omega}(r) = 0, \quad (3.4a)$$

where the effective potential

$$V_{\text{eff}}(r^*, l) = \left[1 - \frac{2M}{r} \right] \left[\frac{2M}{r^3} + \frac{l(l+1)}{r^2} \right] \quad (3.4b)$$

vanishes as $(r^*)^{-2}$ for $r^* \rightarrow \infty$ when $l \neq 0$ and as $\exp(r^*/2M)$ for $r^* \rightarrow -\infty$. The “tortoise distance” $r^* \in (-\infty, +\infty)$ is related to the coordinate $r \geq 2M$ by

$$dr^* = \frac{dr}{1 - 2M/r}, \quad (3.5a)$$

or equivalently

$$r^* = r + 2M \ln(r/2M - 1) + \text{const}. \quad (3.5b)$$

An ambiguity exists in choosing the value of the integration constant (representing the coordinate gauge freedom) appearing in (3.5b). Addition of a constant to r^* that is also l independent amounts to adding a constant to each of the phase shifts and will not affect the summed differential cross section. Because of the freedom inherent in choosing the constant, we pick a value that will equate the numerically computed phase shift to its Newton equivalent for some predetermined large l . This allows us to compute only a few phase shifts numerically before matching onto the Newton analytic solutions for the higher l values [10].

As $r \rightarrow \infty$ (or equivalently as $r^* \rightarrow \infty$) Eq. (3.4) has approximate solutions $r R_{l\omega} \sim \exp(\pm i\omega r^*)$. The logarithmic phase shift at large r suggests that a *distorted* plane wave approximation be made even at great distances. The asymptotic ($r \rightarrow \infty$) form of the distorted plane wave is given by [1,11]

$$\phi \sim \sum_{l=0}^{\infty} \frac{(2l+1)}{2i\omega r} [e^{i\omega r^*} - (-1)^l e^{-i\omega r^*}] P_l(\cos\theta) e^{-i\omega t}. \quad (3.6)$$

The corresponding asymptotic solution to the radial equation (3.4) for each partial wave has the analytic form

$$r R_{l\omega}(r) \sim \frac{2l+1}{2i\omega} [e^{i\omega r^*} e^{2i\delta_l} - (-1)^l e^{-i\omega r^*}], \quad (3.7)$$

where δ_l is the Schwarzschild phase shift between the outgoing and incoming waves determining the scattering amplitude. Explicit use of this analytic form will be made in extracting phase shifts from the numerical solutions. This procedure is described in detail in the next section.

The different scattering cross section is defined as [10,12]

$$\frac{d\sigma}{d\Omega} = |f(\theta)|^2, \quad (3.8)$$

where

$$f(\theta) = \frac{1}{2i\omega} \sum_{l=0}^{\infty} (2l+1) (e^{2i\delta_l} - 1) P_l(\cos\theta) \quad (3.9)$$

is the scattering amplitude given in terms of the phase shift δ_l .

B. Numerical methods

In numerically solving (3.4), one must first specify the proper boundary conditions. Because the effective potential $V_{\text{eff}}(r^*, l)$ vanishes exponentially as $r^* \rightarrow -\infty$ (or

$r \rightarrow 2M$), there is no backscattering from negative values of r^* for a pulse of scalar radiation incident from $r^* = +\infty$ [10,12]. As a result, the pulse will be purely ingoing at the Schwarzschild horizon $r = 2M$ and we take for boundary conditions that $rR_{l\omega}(r) = \exp(-i\omega r^*)$ at $r^* = -30M$ for each partial wave. The exponential vanishing of $V_{\text{eff}}(r^*, l)$ at negative r^* implies that the choice $r^* = -30M$ makes $V_{\text{eff}}(r^*, l)$ very nearly zero and, for computational purposes, the specified boundary conditions are appropriate solutions to (3.4).

The second-order ordinary differential equation (3.4) can be reduced to two first-order equations:

$$\frac{d(rR_{l\omega})}{dr^*} = u(r^*), \quad (3.10a)$$

$$\frac{du(r^*)}{dr^*} = - \left[\omega^2 - \left(1 - \frac{2M}{r} \right) \left(\frac{2M}{r^3} + \frac{l(l+1)}{r^2} \right) \right] rR_{l\omega}, \quad (3.10b)$$

where $u(r^*)$ is a new variable defining the first derivative of $rR_{l\omega}$. Because the wave variables are complex, Eqs. (3.10) represent four coupled first-order differential equations. The real and imaginary parts each obey independent differential equations.

The problem is now posed as a generic situation involving the study of N coupled first-order differential equations. Runge-Kutta methods are particularly suited to such problems and we rely on a fourth order Runge-Kutta scheme [28] to integrate the system (3.10) numerically for $rR_{l\omega}$ and $u(r^*)$ from a boundary near the event horizon to a sufficiently large value of r^* so that the approximation (3.7) is valid. The stopping value of r^* is determined from the condition that the dominant term in the effective potential be $(l^2+1)/r^2 < 10^{-5}$ (the 1 in l^2+1 is introduced for the special case $l=0$). Thus integrations are performed over longer intervals for larger values of l in order to keep errors comparable for different l . This increases the computational time and prevents us from solving for a sequence of arbitrarily large angular momentum wave functions.

Equations (3.10) are transcendental in the sense that the independent variable is r^* but it appears only indirectly in (3.10) through the variable r defined by (3.5b). It is therefore necessary to solve (3.5b) for r at every integration step in r^* . We solve, for the roots of the function,

$$r + 2M \ln \left(\frac{r}{2M} - 1 \right) - r^* = 0, \quad (3.11)$$

for r using a bisection method [28] at every integration step r^* . Notice that the integration constant in (3.5b) has been set to zero. The actual value is unimportant at this stage but it will be computed indirectly when the Schwarzschild and Newton phase shifts are matched at some l . Because (3.11) is a monotonic or single-valued function [see Fig. 2(b)], we encounter no difficulties in finding roots. In fact, the method converges rapidly enough that solving (3.11) at each step of the integration does not appreciably increase the computational time.

As mentioned in the previous section, at sufficiently large r^* , one expects the analytic form (3.7) to hold. Assuming such a linear superposition of incoming and outgoing waves, we represent the numerical solution for $rR_{l\omega}$ as

$$Y = Ae^{i\omega r^*} + Be^{-i\omega r^*}, \quad (3.12a)$$

and, for $u(r^*)$,

$$\dot{Y} = i\omega Ae^{i\omega r^*} - i\omega Be^{-i\omega r^*}, \quad (3.12b)$$

where $Y \equiv Y_R + iY_I$ and $\dot{Y} \equiv dY/dr^* \equiv \dot{Y}_R + i\dot{Y}_I$. Also, the amplitudes $A \equiv A_R + iA_I$ and $B \equiv B_R + iB_I$ are complex numbers independent of r^* and defined by the inverse of Eqs. (3.12):

$$A_R = \frac{1}{2} \left[Y_R + \frac{\dot{Y}_I}{\omega} \right] \cos \omega r^* + \frac{1}{2} \left[Y_I - \frac{\dot{Y}_R}{\omega} \right] \sin \omega r^*, \quad (3.13a)$$

$$A_I = \frac{1}{2} \left[Y_I - \frac{\dot{Y}_R}{\omega} \right] \cos \omega r^* - \frac{1}{2} \left[Y_R + \frac{\dot{Y}_I}{\omega} \right] \sin \omega r^*, \quad (3.13b)$$

$$B_R = \frac{1}{2} \left[Y_R - \frac{\dot{Y}_I}{\omega} \right] \cos \omega r^* - \frac{1}{2} \left[Y_I + \frac{\dot{Y}_R}{\omega} \right] \sin \omega r^*, \quad (3.14a)$$

$$B_I = \frac{1}{2} \left[Y_I + \frac{\dot{Y}_R}{\omega} \right] \cos \omega r^* + \frac{1}{2} \left[Y_R - \frac{\dot{Y}_I}{\omega} \right] \sin \omega r^*. \quad (3.14b)$$

The real and imaginary components of Y and \dot{Y} are obtained directly from the Runge-Kutta integrator since $Y \equiv rR_{l\omega}$ and $\dot{Y} \equiv u(r^*)$. Hence, the right-hand sides of Eqs. (3.13) and (3.14) are known numerically so that the wave amplitudes A and B can be constructed easily.

A direct comparison to the expected analytic solution (3.7) can now be made. Simplifying the notational form of (3.7), we rewrite it as

$$rR_{l\omega}(r) = \frac{(2l+1)W}{2i\omega} [Xe^{i\omega r^*} - (-1)^l e^{-i\omega r^*}], \quad (3.15)$$

where

$$X \equiv X_R + iX_I = e^{2i\delta_l} \quad (3.16)$$

is the complex phase shift and $W = W_R + iW_I$ is introduced as a complex proportionality constant. The constant W is found by equating the incoming part of the numerical solution Y in (3.12) to the incoming part of the analytic form for $rR_{l\omega}(r)$ in (3.15). This results in

$$W_R = \frac{2\omega B_I}{(2l+1)(-1)^l}, \quad (3.17)$$

$$W_I = -\frac{2\omega B_R}{(2l+1)(-1)^l}. \quad (3.18)$$

Similarly, we set the outgoing part of Y equal to the outgoing part of $rR_{l\omega}$, obtaining

$$X_R = \frac{2\omega(A_R W_I - A_I W_R)}{(2l+1)(W_I^2 + W_R^2)}, \quad (3.19a)$$

$$X_I = \frac{2\omega(A_I W_I + A_R W_R)}{(2l+1)(W_I^2 + W_R^2)}. \quad (3.19b)$$

Expressions (3.19) define the real and imaginary parts of the phase shift in terms of quantities readily determined from the numerical solution.

The scattering amplitude $f(\theta)$ is defined by Eq. (3.9). Unfortunately, the infinite sum does not converge rapidly enough to allow a direct numerical computation. However, for $l > L$ (where L is an integer dependent on $M\omega$) the Schwarzschild phase shift δ_l approaches the phase shift η_l for the equivalent Newton problem [1]. Taking advantage of this, the procedure is to sum the finite series for the first L terms in (3.9) then approximate the remaining contribution by the equivalent Newton terms which have an analytic form. The value of L is determined from accuracy and computational time considerations. A larger L results in substantially longer run times and more accurate solutions. However, the accuracy of solutions saturates beyond a certain value of L and an optimal choice for L can be made experimentally. We discuss this point further in the next section.

The Newton phase shift is given by [10,12]

$$\eta_l = -\arg \Gamma(l+1+2iM\omega) \quad (3.20a)$$

or

$$e^{2i\eta_l} = \frac{\Gamma(l+1-2iM\omega)}{\Gamma(l+1+2iM\omega)}. \quad (3.20b)$$

Because we need to match the Schwarzschild phase shifts onto the Newton phases at $l=L$, the form (3.20a) is the more appropriate since it details directly with η_l . For computational purposes we replace the gamma function in (3.20a) by the identity

$$\arg \Gamma(x+iy) = y\psi(x) + \sum_{n=0}^{\infty} \left[\frac{y}{x+n} - \arctan \frac{y}{x+n} \right], \quad (3.21)$$

where $\psi(x)$ is the psi function defined as the logarithmic derivative of $\Gamma(x)$ or equivalently as

$$\psi(n) = -\gamma + \sum_{k=1}^{n-1} k^{-1}, \quad (3.22)$$

where $\gamma = -\psi(1) = 0.577 \dots$ is Euler's constant. Equations (3.20a), (3.21), and (3.22) together define the Newton phase shifts in a form that is convenient for numerical calculations. The series (3.21) can be truncated to any desired accuracy.

The total or summed Newton scattering amplitude is given by [10]

$$g(\theta) = M e^{2i\eta_0} (Z^{2iM\omega}/Z), \quad (3.23)$$

where

$$Z = \sin^2(\theta/2), \quad (3.24)$$

and

$$Z^{2iM\omega} = \exp\{2iM\omega \ln[\sin^2(\theta/2)]\}. \quad (3.25)$$

Consequently, the Schwarzschild cross section (3.8) can be written as

$$\frac{d\sigma}{d\Omega} = \left| g(\theta) - \frac{1}{2i\omega} \sum_{l=0}^L (2l+1)(e^{2i\eta_l} - 1)P_l(\cos\theta) + \frac{1}{2i\omega} \sum_{l=0}^L (2l+1)(X-1)P_l(\cos\theta) \right|^2, \quad (3.26)$$

where we have already noted that $X = \exp(2i\delta_l)$ is the complex phase shift obtained from the numerical solution by Eqs. (3.19). The first two terms in (3.26) give the contribution of partial waves with angular momentum $L+1 \leq l \leq \infty$ to the Newton scattering amplitude which, for sufficiently large L , is approximately equivalent to the Schwarzschild result for the same l values.

The matching of δ_l to η_l at $l=L$ is accomplished by computing δ_L numerically, then adding the difference $c = \eta_L - \delta_L$ to all the δ_l for $l \leq L$. In terms of numerically computed quantities, we have

$$\delta_{IR} = \frac{1}{2} \arctan \left[\frac{X_I}{X_R} \right] + c, \quad (3.27a)$$

$$\delta_{II} = -\frac{1}{4} \ln(X_I^2 + X_R^2) \quad (3.27b)$$

for the real and imaginary parts of δ_l . Notice that since there is no absorption in the Newton problem, the imaginary parts of η_l are zero and we need only correct the real part of δ_l . We have verified that δ_{II} do indeed vanish for the larger l . Also, because a computer calculates only the principal values of $\arctan(x)$ which lie between $-\pi/2 \leq \arctan(x) \leq \pi/2$, care must be taken to place δ_l in the proper quadrant before adding c . The sum (3.26) is performed with the corrected phase shifts.

C. Code tests and results

We have subjected our code to a number of tests designed to check the reliability and accuracy of numerical solutions. First, the accuracy of the fourth-order Runge-Kutta integrator was tested against the analytic solution $rR_{00} = r$ to the s -wave radial equation [$l=0$ in (3.4)] with $\omega=0$. We have verified that the numerical solution converges to the analytic solution as the truncation error $(\Delta r^*)^4$ of the fourth-order method.

Other tests include actual computations of cross sections. Direct comparisons can be made in some limits that allow analytic approximations. For example, at small scattering angles we expect to recover the forward divergence of the Newtonian formula for the summed differential scattering cross section [1]

$$\frac{d\sigma}{d\Omega} = \frac{M^2}{\sin^4(\theta/2)}. \quad (3.28)$$

At small angles ($\theta \sim 0.01\pi$), relative differences between the Newtonian formula (3.28) and our numerical results

are less than half of a percent. The analytic glory scattering cross section for spin-0 scalar waves provides another code test for scattering angles near $\theta \approx \pi$. The analytic form of this behavior is approximated by [3,4]

$$\left. \frac{d\sigma}{d\Omega} \right|_{\text{glory}} = 2\pi\omega B^2 \left| \frac{dB}{d\theta} \right| J_0^2(\omega B \sin \theta), \quad (3.29a)$$

where

$$B = (3\sqrt{3} + 3.48e^{-\theta})M \quad (3.29b)$$

is the glory impact parameter and J_0 is a Bessel function. In Fig. 6 we present a graphic comparison of our numerical results (solid line) to the analytic approximation (dashed line). We plot the cross section versus scattering angle (in units of π) for the case $\omega=2.5$, $M=1$ and $L=60$. The match is excellent for $\theta \approx \pi$.

Together, the previous two tests provide checks on small and large angle scattering and suggest that the methods we use are accurate enough to solve for cross sections over the entire range of scattering angles. An additional check can be made by verifying that our solutions converge for larger values of l . In Fig. 7 we show the summed cross section for $L=20$ (short dashed line), $L=40$ (long dashed line) and $L=60$ (solid line) with $\omega=2.5$ and $M=1$. It is clear that computation of the first twenty partial wave contributions resolves the qualitative features of the larger scattering angles but fails for the smaller angles. However, the series quickly converges for higher L , with $L=40$ and $L=60$ yielding nearly identical cross sections.

Finally, we verified that our solutions are affected neither by decreasing the integration step nor by our choice

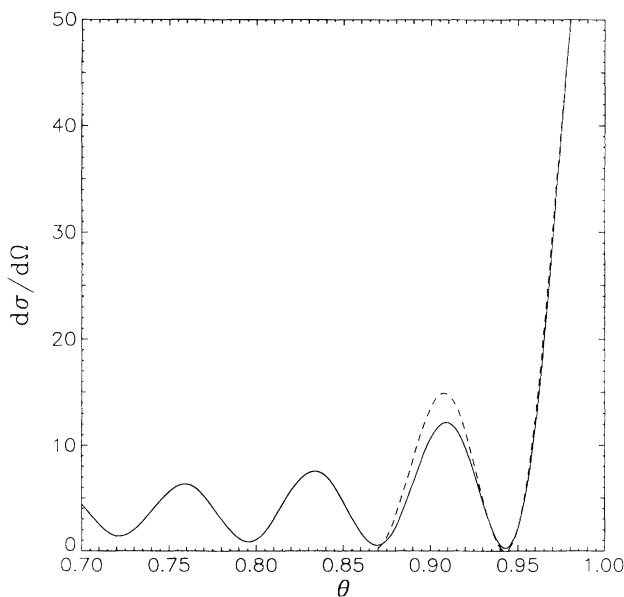


FIG. 6. As Fig. 1 except the cross section presented here is for the scattering of scalar waves with $M\omega=2.5$. The scattering angle θ is displayed in fractions of π . The dashed line is the analytic glory scattering cross section and the solid line is the numerical cross section.

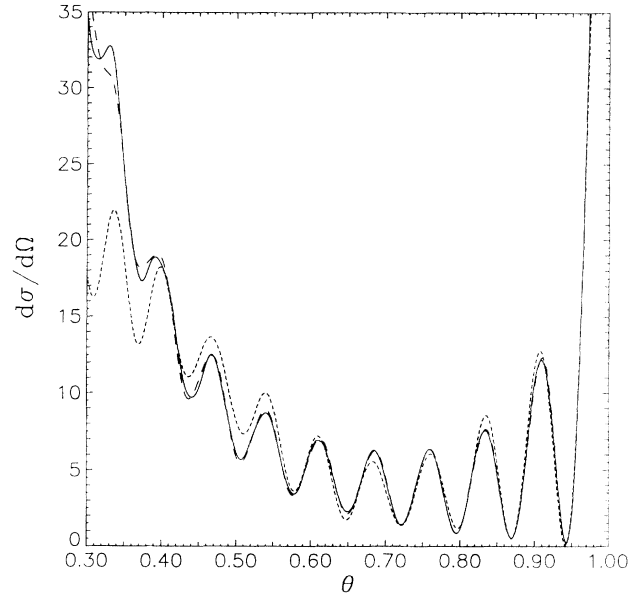


FIG. 7. A convergence test on the numerical computation of the scattering cross section. The short dashed line corresponds to all l up to and including $L=20$, the long dashed line is $L=40$ and the solid line represents $L=60$. For $l > L$, the amplitude is approximated by the corresponding Newtonian amplitude. Henceforth all calculations are done with $L=60$.

in locating the starting and terminal r^* (that is by the choice of asymptotic negative and positive infinity, respectively). In summary, all code tests performed indicate that our numerical solutions are accurate. Having established this fact, we now proceed to investigate orbital scattering (orbiting) in more detail.

Figure 6 demonstrates that behavior in $d\sigma/d\Omega$ near $\theta \approx \pi$ in the differential cross section are explained as glory scattering interference. The analytic result (2.67) in Sec. II is an approximation to the cross section when one considers orbital scattering and is valid for intermediate scattering angles θ . Together, glory and orbital scattering may provide a complete physical interpretation of the oscillatory behavior in the cross section for a wide range of scattering angles. Comparison of the analytic orbiting cross sections to numerical solutions is presented in Fig. 9. Before discussing these results, we point out that the numerical solutions these figures include absorption. However, the analytic solution was derived from considerations of angular momentums $l > \bar{l} = 3\sqrt{3}M\omega$ and thus ignores absorption. This difference can easily be compensated for in the numerical solutions for $M\omega=2.5$ by simply neglecting the first thirteen ($\bar{l} = 3\sqrt{3}M\omega \approx 13$) terms in the Schwarzschild scattering amplitude when computing the cross section from (3.26). We plot this result in Fig. 8 with a dashed line and compare it to the case which includes absorption (solid line). It is clear that the contribution due to absorption is negligible.

The orbital scattering formula (dashed line) is shown in Fig. 9 for the case $\omega=2.5$ and $M=1$ along with the cor-

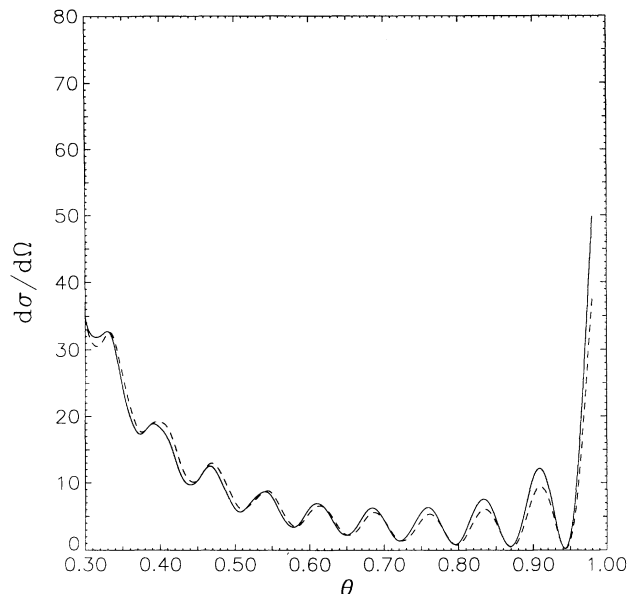


FIG. 8. Testing the importance of the absorption contribution $l < \bar{l}$. The numerical scattering cross section with absorption (solid line) and without absorption (dashed line) is presented for $M\omega = 2.5$. It is evident that absorption does not contribute significantly to the scattering cross section. Note that Fig. 8.1b in Futterman, Handler, and Matzner [10] also shows the partial wave contributions to the total absorption cross section are negligible for large $M\omega$.

responding numerical solution (solid line) with $L = 60$. The oscillatory behavior is the same but for an overall difference in phase and amplitude. This discrepancy was anticipated from the analytic treatment in Sec. II C where the orbital scattering formula was determined up to an overall amplitude $[f(\bar{l})/f(l_0)]$ and an overall phase (Φ). The variables $f(\bar{l})/f(l_0)$ and Φ are chosen to match the analytic with the numerical cross section. The choices $f(\bar{l})/f(l_0) = 8/3$ and $\Phi = \pi$ give a nearly exact fit, as evidenced in Fig. 9.

CONCLUSION

Using partial wave methods, the scattering cross section of scalar waves by a Schwarzschild black hole can be computed numerically for a wide range of scattering angles. Cross sections in the high-frequency limit exhibit an

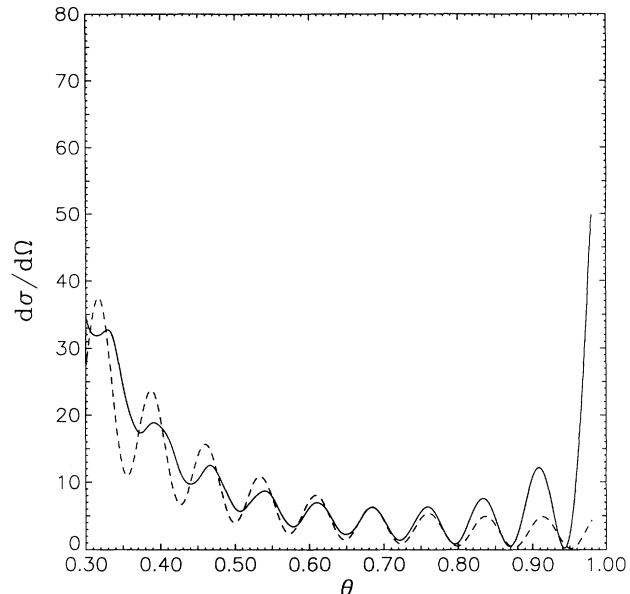


FIG. 9. The analytic orbiting cross section (dashed line) as compared to the numerical solution (solid line) for the case $M\omega = 2.5$ and $L = 60$ in the orbiting region $\theta < 0.9\pi$.

oscillatory dependence on the scattering angle. Previous work has demonstrated via a semiclassical expansion that the oscillations near $\theta = \pi$ are due to glory scattering interference. In this work, we demonstrate that the computed oscillations result from orbital (or spiral) scattering in which waves orbit the black hole before they scatter. Thus, a physical interpretation of scattering can now be given for the entire range of scattering angles.

If rings are ever observed around black holes, the above cross sections will have sharp diagnostic value for the nature of the hole, the nature of the scattered waves, and their wavelength.

Note added in proof. Three articles (N. Sanchez, Phys. Rev. D **18**, 1798 (1978); A. B. Gaina, Zh. Eksp. Teor. Fiz. **98**, 25 (1989) [Sov. Phys. JETP **69**, 13 (1989)]; Class. Quantum Grav. **9**, 667 (1992)) have come to our attention too late to be included in the introduction with other works on orbiting and black hole scattering.

ACKNOWLEDGMENTS

P.A. and R.M. acknowledge support in part by NSF Grant No. PHY8806567.

- [1] K. W. Ford and J. A. Wheeler, Ann. Phys. (N.Y.) **7**, 259 (1959), See Eqs. (3), (41), (44) and discussion following Eq. (44).
- [2] K. W. Ford, D. L. Hill, M. Wakano, and J. A. Wheeler, Ann. Phys. (N.Y.) **7**, 239 (1959). See Eqs. (27) and (29).
- [3] K. W. Ford and J. A. Wheeler, Ann. Phys. (N.Y.) **7**, 287 (1959).
- [4] M. V. Berry, J. Phys. B **2**, 381 (1969).
- [5] F. A. Handler and R. A. Matzner, Phys. Rev. D **22**, 2331 (1980).
- [6] C. DeWitt-Morette and B. L. Nelson, Phys. Rev. D **29**, 1663 (1984).

- [7] T.-R. Zhang and C. DeWitt-Morette, Phys. Rev. Lett. **52**, 2313 (1984).
- [8] For a heuristic calculation see R. Matzner, C. DeWitt-Morette, B. Nelson, and T. R. Zhang, Phys. Rev. D **31**, 1869 (1985).
- [9] For a complete presentation see C. DeWitt-Morette, Acta Phys. Austriaca, Suppl. **XXVI**, 101 (1984). See Table 2, p. 125 for the normalization of the propagator.
- [10] J. A. H. Futterman, F. A. Handler, and R. A. Matzner, *Scattering from Black Holes* (Cambridge University Press, Cambridge, England, 1988), Fig. 8.15.
- [11] C. Darwin, Proc. R. Soc. London **A249**, 180 (1959). See

- Eq. (32) for B_g and bottom of p. 187 for B_{or} .
- [12] R. A. Matzner, *J. Math. Phys.* **9**, 163 (1968).
- [13] F. A. Handler, Ph.D. Dissertation, The University of Texas 1979; see p. 64.
- [14] C. DeWitt-Morette and T.-R. Zhang, *Phys. Rev. D* **28**, 2503 (1983).
- [15] C. DeWitt-Morette and T.-R. Zhang, *Phys. Rev. D* **28**, 2517 (1983).
- [16] C. DeWitt-Morette, B. Nelson, and T. R. Zhang, *Phys. Rev. D* **28**, 2526 (1983).
- [17] C. DeWitt-Morette, A. Maheshwari, and B. Nelson, *Phys. Rep.* **50**, 266 (1979).
- [18] C. DeWitt-Morette, K. D. Elworthy, B. L. Nelson, and G. S. Sammelman, *Ann. Inst. Henri Poincaré* **32**, 327 (1980).
- [19] See, for instance, L. I. Schiff, *Quantum Mechanics* (McGraw-Hill, New York, 1968), pp. 299 and 307–308.
- [20] C. DeWitt-Morette and M. G. G. Laidlaw, *Phys. Rev. D* **3**, 1375 (1971).
- [21] J. S. Dowker, *J. Phys. A* **5**, 936 (1972).
- [22] T. D. Imbo and E. C. G. Sudarshan, *Phys. Rev. Lett.* **60**, 481 (1988).
- [23] T.-R. Zhang, Ph.D. dissertation, University of Texas at Austin, 1985.
- [24] See, for instance, B. S. DeWitt, in *Relativity Groups and Topology*, edited by C. DeWitt and B. DeWitt (North Holland, Amsterdam, 1964). See. p. 739.
- [25] R. P. Feynman, *Phys. Rev.* **80**, 440 (1950). See Appendix A.
- [26] J. Schwinger, *Phys. Rev.* **82**, 664 (1951).
- [27] Y. Choquet-Bruhat and C. DeWitt-Morette, *Analysis, Manifolds, and Physics Part I: Basics* (North Holland, Amsterdam, 1982).
- [28] Williams H. Press, Brian P. Flannery, Saul A. Teukolsky, and William T. Vetterling, *Numerical Recipes: The Art of Scientific Computing* (Cambridge University Press, Cambridge, England, 1986).